Article:
Myhre, G., Hodnebrog, Ø, Loeb, N. et al. (2025) Observed trend in Earth energy imbalance may provide a constraint for low climate sensitivity models. Science, 388 (6752). pp. 1210-1213. ISSN: 0036-8075

https://doi.org/10.1126/science.adt0647

Observed trend in Earth energy imbalance may provide a constraint for low climate sensitivity models

Gunnar Myhre[1]*, Øivind Hodnebrog[1], Norman Loeb[2], Piers M. Forster[3]

[1]CICERO Center for International Climate Research; Oslo, Norway
[2]NASA Langley Research Center, Hampton, VA, USA
[3]Priestley Centre for Climate Futures, University of Leeds, Leeds, UK

*Corresponding author. Email: gunnar.myhre@cicero.oslo.no

Abstract: Climate forcings by greenhouse gases and aerosols cause an imbalance at the top of the atmosphere between the net incoming solar radiation and outgoing longwave radiation from the Earth. This Earth energy imbalance has strengthened over the period 2001-2023 with satellite data. Here, we show that low climate sensitivity models fail to reproduce the trend in Earth energy imbalance, particularly in the individual longwave and shortwave contributions to the imbalance trend. The inability to produce a strong positive shortwave and strong negative longwave Earth energy imbalance trend is found to be a robust feature in the low climate sensitivity models, especially for models with climate sensitivity below 2.5K. The negative longwave contribution to Earth energy imbalance is driven by surface temperature increases and is therefore most pronounced in high climate sensitivity models, whereas the shortwave contribution is generally positive and amplified by greater surface warming.

A long-standing research question in climate science is how sensitive the climate is to increases in greenhouse gases (*1-3*). This climate sensitivity is taken as the surface temperature rise for a doubling of the CO_2 concentration (*4, 5*). In the latest Intergovernmental Panel on Climate Change (IPCC) report the best estimate of the equilibrium climate sensitivity (ECS) was assessed as 3ºC, with a likely range from 2.5ºC to 4ºC and a very likely range from 2ºC to 5ºC (*4*). How clouds change in a warmer world is the main cause of the uncertainty in the climate sensitivity (*4, 5*) with divergent results from observational studies (*6-9*). The recent warming over the first one to two decades in the century has been used as arguments for low climate sensitivity models being most realistic, in particular how feedback processes are represented for recent warming trend (*10, 11*). However, the pattern of observed sea-surface warming in the Pacific may have biased some of these findings (*12*).

The last decades have seen a continued increase in greenhouse gases (GHGs) (*4*) combined with a reversal of the aerosol effect (*13*). A reduction in the cooling effect of aerosols has thus a warming effect and the total effective radiative forcing has been accelerating over the last decades (*14*). The Earth energy imbalance (EEI) is increasing (*15, 16*) and will likely give an accelerated warming over the coming years (*17*). Hodnebrog et al.(*16*) showed that climate models forced with observed sea-surface temperatures reproduce the satellite retrieved strengthening in EEI from the Clouds and the Earth's Radiant Energy System (CERES), but all models have a weaker trend than the observed trend. Schmidt et al (2023) (*18*) showed that the EEI trend split into longwave (LW) and shortwave (SW) trends differed markedly between the CERES satellite and in different configurations of a climate model. Here we use a large set of coupled climate models from the

Coupled Model Intercomparison Project Phase 6 (CMIP6) (*19*) to illustrate that low climate sensitivity models have an EEI trend behaviour that is inconsistent with the satellite derived EEI trend.

Trend in EEI

Fig 1 shows the EEI over the period with CERES satellite data and compared with coupled climate model simulations from CMIP6. The model simulations are a combination of the historical simulation until 2014 combined with a SSP5-8.5 scenario from 2015 onwards. The SSP5-8.5 scenario includes reductions in aerosols combined with a strong increase in GHG concentrations. The CERES data shows a stronger trend in EEI than the multi-model CMIP6 mean and higher EEI in 2023 than any of the CMIP6 models. However, for individual CMIP6 models and ensembles EEI is comparable or higher at other periods than the CERES value in 2023. Interannual variability in EEI is clearly shown for the CERES data and the climate models. In simulations with observed sea-surface temperature, the interannual variability in the CERES data is largely reproduced by the climate models (*16*).

The strengthened EEI from CERES is further supported by an accelerated trend in the ocean heat content (OHC) (*14, 20-22*). Discrepancies exist in the degree of acceleration among various OHC datasets, with best agreement between CERES and OHC datasets having better ocean coverage and filling in data in data sparse regions (*23*).

Relationship of longwave and shortwave EEI trend

To illustrate climate model differences and robustness between models, we use idealized CMIP6 experiments. In Fig 2 the EEI is shown for a range of models for the experiment with 1%/yr increase in CO_2 concentrations (named 1pctCO2). All models show an increasing net EEI (Fig 2a), but with a much larger model diversity when net EEI is split into LW (Fig 2b) and SW EEI (Fig 2c). LW and SW EEI are positive when reducing outgoing radiation at the top of the atmosphere, typically caused by increase in absorption by GHGs (both anthropogenic and as climate feedback). An increase in surface temperature causes an increase in outgoing longwave radiation and thus a negative LW EEI. The majority of models have a negative LW EEI after some years because the increase in surface temperature and more outgoing LW radiation overwhelm the positive effect from the increase in CO_2. However, several models have a positive or very weak LW EEI even after more than 100 years. With one exception, the models have a positive SW EEI mostly throughout the time period of increase in CO_2 caused by less snow and ice (*24*) and contributions from water vapour absorption (*25*) and clouds for several models (see discussions in next sections). Fig 2d shows trend in LW EEI versus SW EEI for the CMIP6 models with uncertainties reflecting variation among four 23-year periods over the model simulations. Consistent with Schmidt et al (2023) (*18*), we find a robust linear relationship in the LW and SW EEI trends amongst model members and a marked spread in the trends. Periods of 23 years are selected to match the length of data available from CERES.

Linking trends in EEI with climate sensitivity

Fig 3a shows the 1pctCO2 experiment and the abrupt quadrupling of CO_2 (abrupt4xCO2) experiment with colours reflecting the ECS. The LW and SW EEI trends are calculated as a mean of four 23-year trends and ECS from regressions using the abrupt4xCO2 experiment over 150 years (*26*) and thus consistent with ECS values derived elsewhere (*4, 27*). The 1pctCO2 and abrupt4xCO2 experiments show different trend relationships for LW and SW EEI with the former having weaker LW negative trend gradient as a sustained increase in CO_2 contributes to LW EEI

imbalance. The shading in Fig 3a shows that the net EEI is generally increasing in the 1pctCO2 experiment and decreasing in the abrupt4xCO2 experiment. Fig 3a also includes atmosphere-only simulations with observed sea-surface temperature (SST) fields from 2001 to 2019 from Hodnebrog et al. (*16*). Atmosphere-only simulations where climate drivers (GHGs and aerosols) have been kept constant for the period 2001-2019 align with the abrupt4xCO2 experiment, and atmosphere-only simulations with increase in GHG (but constant aerosols) over the 2001-2019 period show similar LW and SW trends as the 1pctCO2 experiment. Importantly, the low climate sensitivity models have much weaker changes in LW and SW EEI trends than the other models. In particular, the models with ECS below 2.5 K all show very weak LW and SW EEI trends. For models with ECS 4 K or higher, there is little alignment with the LW and SW EEI trends, and the models are widely spread along the regression line. Nevertheless, it is notable that none of these models show very weak LW and SW EEI trends.

In Fig 3b the CERES satellite LW and SW EEI trend is shown together with the CMIP6 intra-model ensemble mean LW and SW EEI trend for the period 2001 to 2023. CMIP6 simulations are from a combination of the historical simulation until 2014 and the SSP5-8.5 scenario from 2015. Results are very similar for other scenarios with aerosol reductions (e.g. SSP2-4.5). Additionally, atmosphere-only simulations with changes in GHG and aerosols from Hodnebrog et al (*16*) are included in Fig 3b, note that these are for 2001-2019. The number of ensemble members for each model is quite variable, see Supplementary Table 1. Fig 3c shows results for all ensemble members included in this study. Fig 3b and Fig 3c show systematic weak LW and SW EEI trends from low climate sensitivity models, consistent with Fig 3a. Note, that the relationship between climate sensitivity and net EEI trends show no systematic pattern, and various intra-model ensemble members exhibit a wide range in the net EEI trend (Supplementary Fig 1). All models with climate sensitivity below 2.5K have very weak LW and SW EEI trends. It is worth mentioning some of the EEI trends of lighter colours in Fig 3b and Fig 3c. FGOALS-f3-l has a LW EEI trend similar to CERES and SW EEI trend 0.2 W m-2/decades weaker than CERES, but this is a model with climate sensitivity of 3.0 K (see Fig 3b). In Fig 3c one ensemble member out of 50 for MIROC6 has a SW EEI trend above 0.4 W m-2/decades. MIROC6 has a climate sensitivity of 2.6 K. GISS-E2-2-G is among the very low climate sensitivity models with ECS of 2.4 K and has one out of five ensemble members with SW EEI trend above 0.4 W m-2/decades (0.41) but with a near zero LW EEI. The atmosphere only simulations in Fig 3b are closer to CERES LW and SW EEI trends than the fully coupled simulations of the same model. This can be illustrated by HadGEM3, which shows slightly weaker trends than CERES where observed sea-surface temperature is used, and much stronger trends in the coupled simulations. Similarly, NorESM2 aligns better with CERES data when using observed sea-surface temperatures simulations, showing stronger LW and SW EEI trends than in fully coupled simulations. However, differences with CERES are also evident among model simulations using observed sea-surface temperatures, indicating that both the atmospheric and ocean components of the climate models contribute to differences in the LW and SW EEI trends.

Clear sky LW and SW EEI trends show similar patterns to all sky with strong negative LW EEI trends for high climate sensitivity models and positive SW EEI trends in idealized CMIP6 experiments (see Supplementary Figure 2). The largest difference between the clear sky and all sky results are for SW EEI trends (see Figure 3a and Supplementary Figure 2).

EEI trends and surface warming

The surface temperature warming differs substantially between the CMIP6 models, and Figure 4 (and Supplementary Figure 3 and Supplementary Figure 4) investigates if this alters the

relationships shown in Figure 3. The most striking result is that the CERES data show higher SW EEI trend per degree warming than any of the CMIP6 models, and only the models with strong negative LW EEI trend per degree warming are close to CERES (Figure 4). The low climate sensitivity models have consistently much weaker LW and SW EEI trends per degree warming than the CERES data.

Discussion

The analysis above relates to models' long-term climate sensitivity estimated from abrupt 4xCO2 experiments. This can differ from their effective climate sensitivity, estimated from changes over the recent historical period. Previous studies find that climate models are unable to capture the recent pattern of East Pacific warming observed (*28*), and this is associated with reduced effective feedbacks and reduced effective climate sensitivity (*12*).. Hodnebrog et al. (*16*) find that applying SST patterns to models improve EEI trends across models. Comparing the observed SST simulations (triangles) to their coupled modelled counterparts (circles) in Figure 3b, low sensitivity models such as NorESM exhibit relatively modest differences in the EEI trends and remain well below the CERES trend even with the observed SST pattern applied. Hence the particular observed SST pattern is unlikely to play a large role for the low climate sensitivity models substantially underestimating the LW EEI and SW EEI trends compared to CERES.

Climate models consistently show a robust feature of a relationship between LW EEI and SW EEI trends which varies depending on climate drivers involved in the simulations (Fig 3a and 3b). This relationship is also evident under clear sky conditions (see Supplementary Figure 2), where the positive SW EEI trend often is modest and driven by reduced surface albedo from less snow and ice in addition to contributions from SW absorption by water vapour. The negative LW EEI trend is driven by surface temperature increase and moderated if GHGs are increasing during the simulations. Cloud changes further amplify the clear-sky relationship between LW EEI and SW EEI trends. Supplementary Figure 5 shows previously derived SW and LW cloud feedbacks (*27*) which exhibit a similar shape of relationship to that of LW EEI and SW EEI trends, but slightly different gradient. Notably, SW cloud feedback demonstrates greater model diversity than LW cloud feedback, although the latter also shows substantial variability. A negative correlation between LW and SW cloud feedbacks can be expected due to the opposing warming and cooling effect of clouds on the climate system (*29*).

We show, using a large set of climate models, that trend in net EEI has no clear relationship to climate sensitivity. Consequently, we argue that the trends in net EEI and surface warming trend over the first two decades of this century provide little constraint on climate sensitivity. However, we present robust findings for trends in LW and SW EEI. These trends, and their relationship to climate sensitivity, are more physically based than the net EEI trend. The model distribution of EEI trends compared to CERES is shown in Supplementary Figure 6. All models, given as the 99.999% level of the distribution, with an ECS of 2.93 K or below are outside the CERES range. The models have a similar positive aerosol radiative forcing trend as that observed, around 0.16 Wm^{-2} per decade (*16, 31*). This would need to be underestimated by at least 50% to make the SW EEI trend from models with an ECS of 2.5 K match the CERES range, making such a low ECS unlikely.

Methods

All trends of EEI and surface temperatures are linear trends between 2001 and 2023, inclusive. The model climate sensitivity is derived by regression of model EEI and surface temperature change in CMIP6 abrupt 4xCO_2 simulations after 150 years (*26*), usually denoted as effective climate sensitivity (*4*). Uncertainties in the EEI CERES data are derived as in Loeb et al. (*23*). In Figure 4 the LW and SW EEI per degree of warming is derived by regression of LW/SW EEI against the temperature trend.

Funding: The European Union's Horizon 2020 research and innovation programme under grant agreement 820829 (CONSTRAIN) (GM, ØH, PMF) and project grants no. 325270 by the Norwegian Research Council (GM, ØH).

Author contributions:

Conceptualization: GM

Methodology: GM, ØH, NL, PMF

Investigation: GM, ØH, NL, PMF

Formal analysis: GM

Visualization: GM

Validation: GM, ØH, NL, PMF

Writing – original draft: GM

Writing – review & editing: GM, ØH, NL, PMF

Competing interests: Authors declare that they have no competing interests.

Data and materials availability: CMIP6 model data used in this study are freely available from the CMIP6 repository on the Earth System Grid Federation nodes (https://esgf-node.llnl.gov/search/cmip6/, World Climate Research Programme, 2020). Derived LW and SW EEI from CMIP6 data presented in Fig 3b,c are available at Zenodo, https://doi.org/10.5281/zenodo.15087491. CERES EBAF-TOA Edition4.2 data were obtained from the NASA Langley Research Centre CERES ordering tool at https://ceres.larc.nasa.gov/data/. GISTEMP Team, 2024: *GISS Surface Temperature Analysis (GISTEMP), version 4*. NASA Goddard Institute for Space Studies. Dataset accessed 2024-07-05 at https://data.giss.nasa.gov/gistemp/. Results for observed sea-surface temperature simulations are from Hodnebrog et al. (*16*).

Figures:

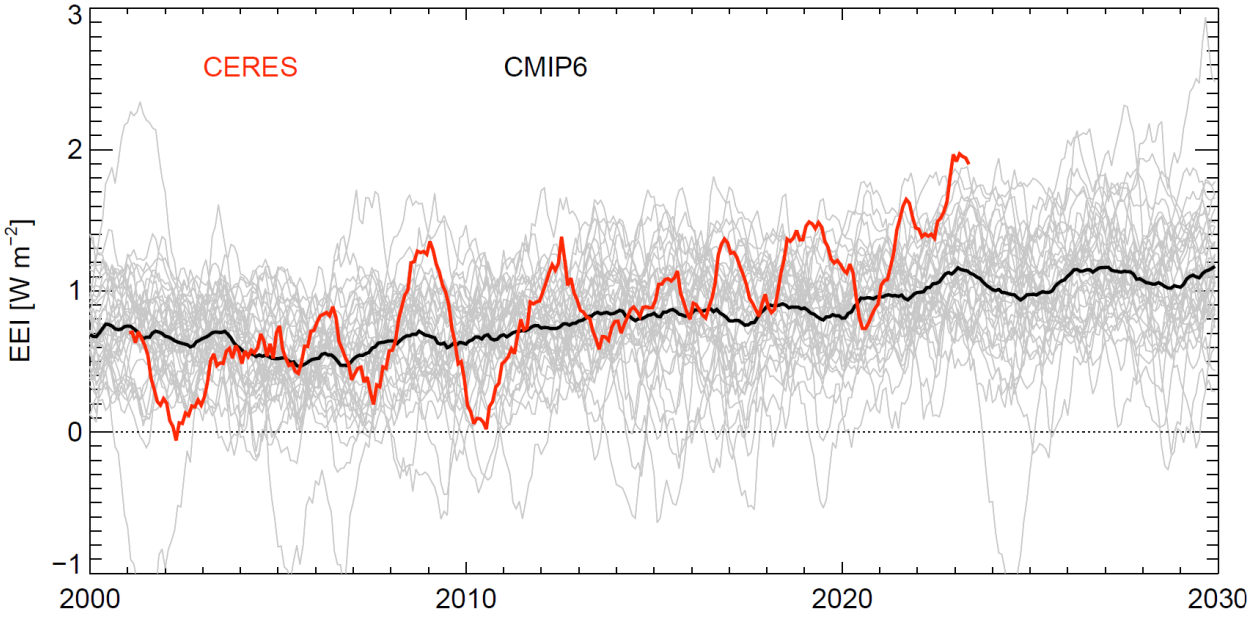

Fig. 1. Trend in EEI in CERES and CMIP6 models. The CERES data is shown from 2001 to 2023. The CMIP6 data is shown 2000-2030. All EEI are given as 12-month running means. CMIP6 model mean is shown by a black thick line and individual models in thin grey lines. Only one ensemble member for each of the models is shown.

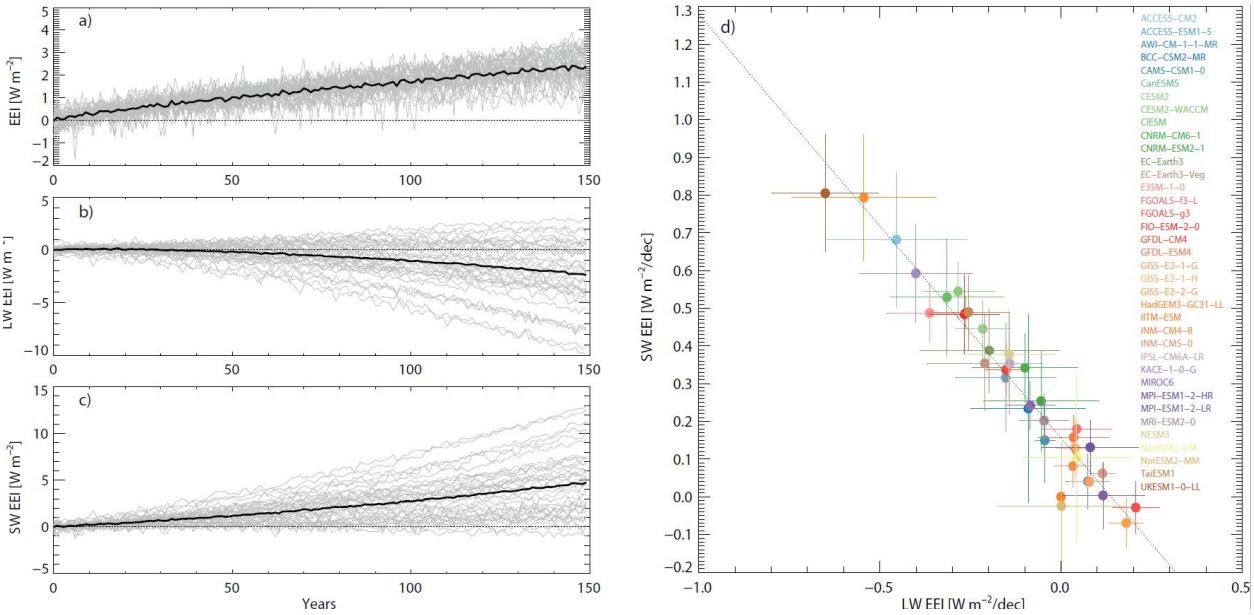

Fig. 2. EEI in CMIP6 models of 1%/year increase in CO_2 (1pctCO2). Net EEI a), LW EEI b), SW EEI c) and SW EEI versus LW EEI trends where trends are derived from four 23-year intervals d). Uncertainty ranges shown in Fig 2d represent the standard deviation among the four 23-year intervals.

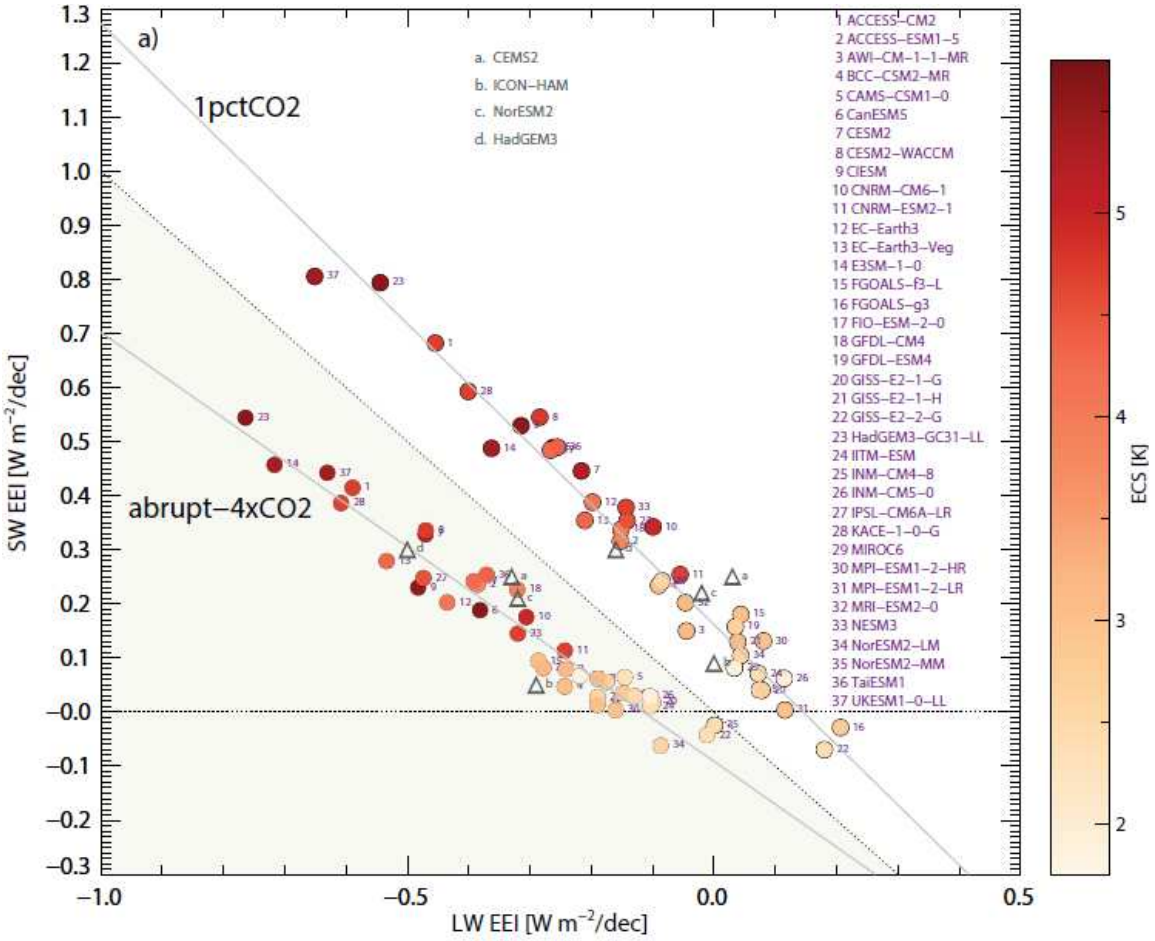
a)
1pctCO2
abrupt−4xCO2
a. CEMS2
b. ICON−HAM
c. NorESM2
d. HadGEM3
1 ACCESS−CM2
2 ACCESS−ESM1−5
3 AWI−CM−1−1−MR
4 BCC−CSM2−MR
5 CAMS−CSM1−0
6 CanESM5
7 CESM2
8 CESM2−WACCM
9 CIESM
10 CNRM−CM6−1
11 CNRM−ESM2−1
12 EC−Earth3
13 EC−Earth3−Veg
14 E3SM−1−0
15 FGOALS−f3−L
16 FGOALS−g3
17 FIO−ESM−2−0
18 GFDL−CM4
19 GFDL−ESM4
20 GISS−E2−1−G
21 GISS−E2−1−H
22 GISS−E2−2−G
23 HadGEM3−GC31−LL
24 IITM−ESM
25 INM−CM4−8
26 INM−CM5−0
27 IPSL−CM6A−LR
28 KACE−1−0−G
29 MIROC6
30 MPI−ESM1−2−HR
31 MPI−ESM1−2−LR
32 MRI−ESM2−0
33 NESM3
34 NorESM2−LM
35 NorESM2−MM
36 TaiESM1
37 UKESM1−0−LL
SW EEI [W m−2/dec]
LW EEI [W m−2/dec]
ECS [K]

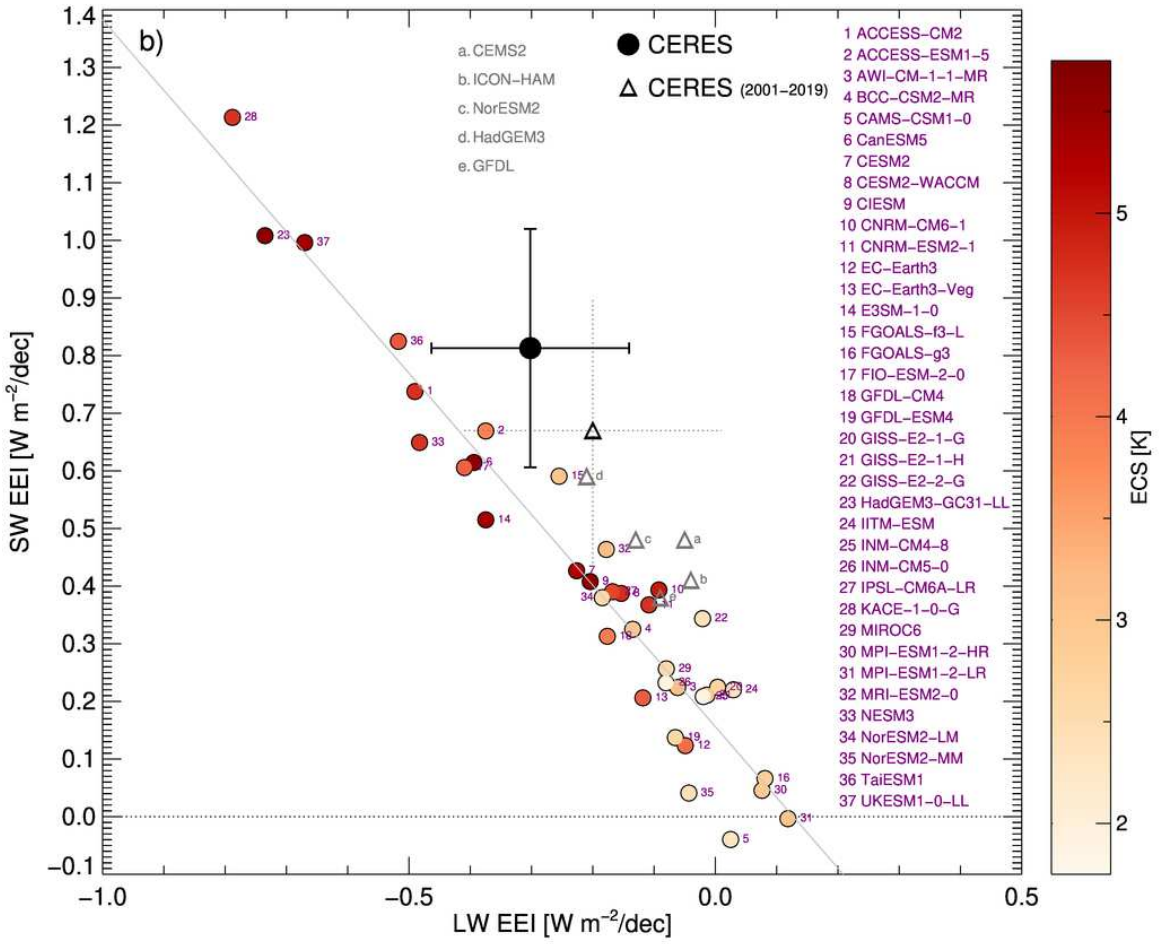
b)
a. CEMS2
b. ICON–HAM
c. NorESM2
d. HadGEM3
e. GFDL
CERES
CERES (2001–2019)
1 ACCESS–CM2
2 ACCESS–ESM1–5
3 AWI–CM–1–1–MR
4 BCC–CSM2–MR
5 CAMS–CSM1–0
6 CanESM5
7 CESM2
8 CESM2–WACCM
9 CIESM
10 CNRM–CM6–1
11 CNRM–ESM2–1
12 EC–Earth3
13 EC–Earth3–Veg
14 E3SM–1–0
15 FGOALS–f3–L
16 FGOALS–g3
17 FIO–ESM–2–0
18 GFDL–CM4
19 GFDL–ESM4
20 GISS–E2–1–G
21 GISS–E2–1–H
22 GISS–E2–2–G
23 HadGEM3–GC31–LL
24 IITM–ESM
25 INM–CM4–8
26 INM–CM5–0
27 IPSL–CM6A–LR
28 KACE–1–0–G
29 MIROC6
30 MPI–ESM1–2–HR
31 MPI–ESM1–2–LR
32 MRI–ESM2–0
33 NESM3
34 NorESM2–LM
35 NorESM2–MM
36 TaiESM1
37 UKESM1–0–LL
SW EEI [W m^{-2}/dec]
LW EEI [W m^{-2}/dec]
ECS [K]

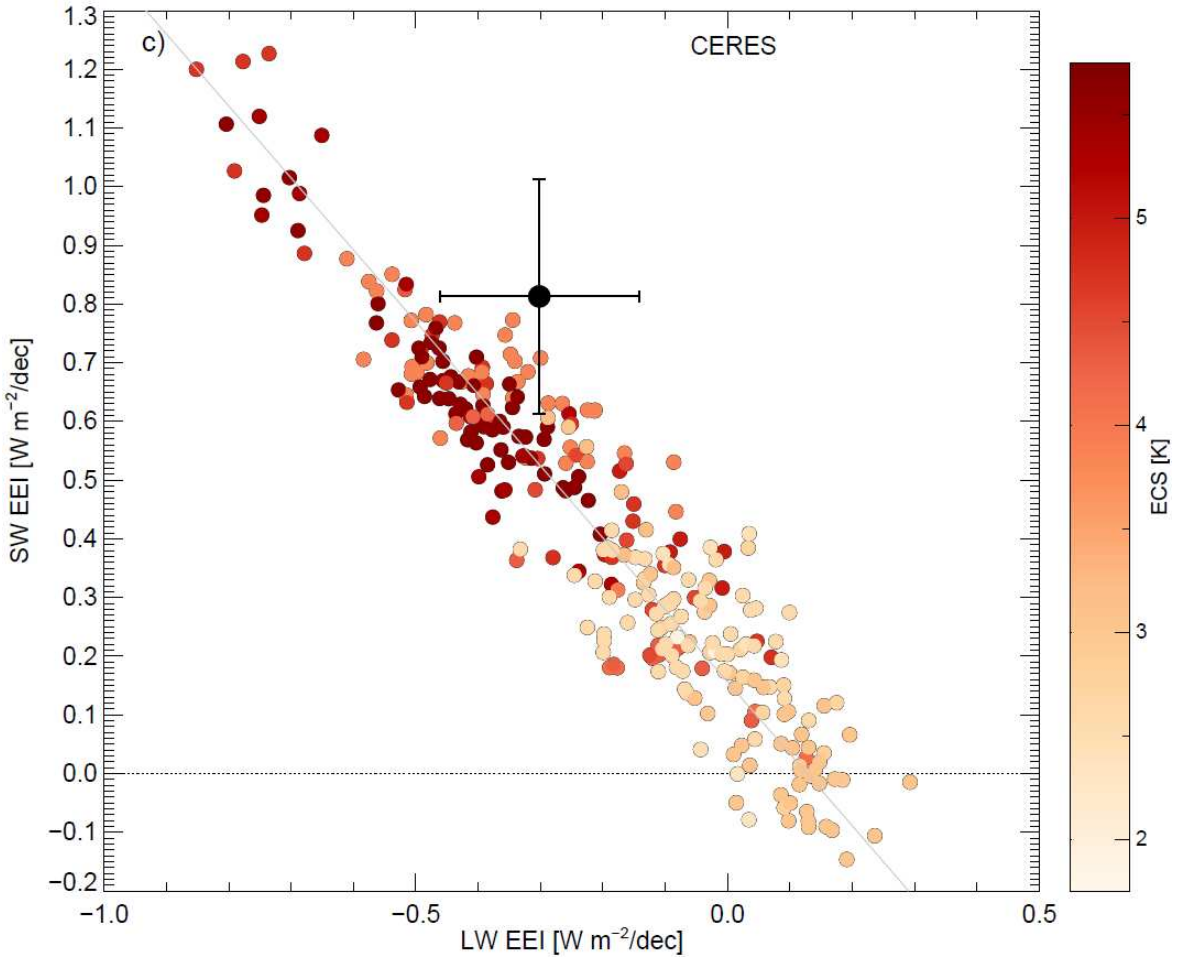

Fig. 3. SW EEI versus LW EEI trends and their relation to climate sensitivity in CMIP6 models. Primary ensemble member from each CMIP6 model for the abupt-4xCO2 and 1%/yrCO2 experiments with results from Hodnebrog et al. (*16*) on all driver constants (following abupt-4xCO2) and only GHG changes included (following 1%/yrCO2) a), CERES and ensemble mean from each CMIP6 models (historical+SSP5-8.5) for 2001-2023 with results from Hodnebrog et al. (*16*) shown in grey colours for the period 2001-2019 (see further description in Supplementary text) b), and CERES and all individual ensemble members from CMIP6 models for 2001-2023 c). The range of ECS in the CMIP6 models is from 1.9 K to 5.6 K. In panel a) the 1pctCO2 simulations have thicker lines around the circles than the abrupt-4xCO2 simulations. Yellow-grey shaded area in panel a) shows where net EEI trend is negative. Lines around the CERES trends are 90% confidence intervals.

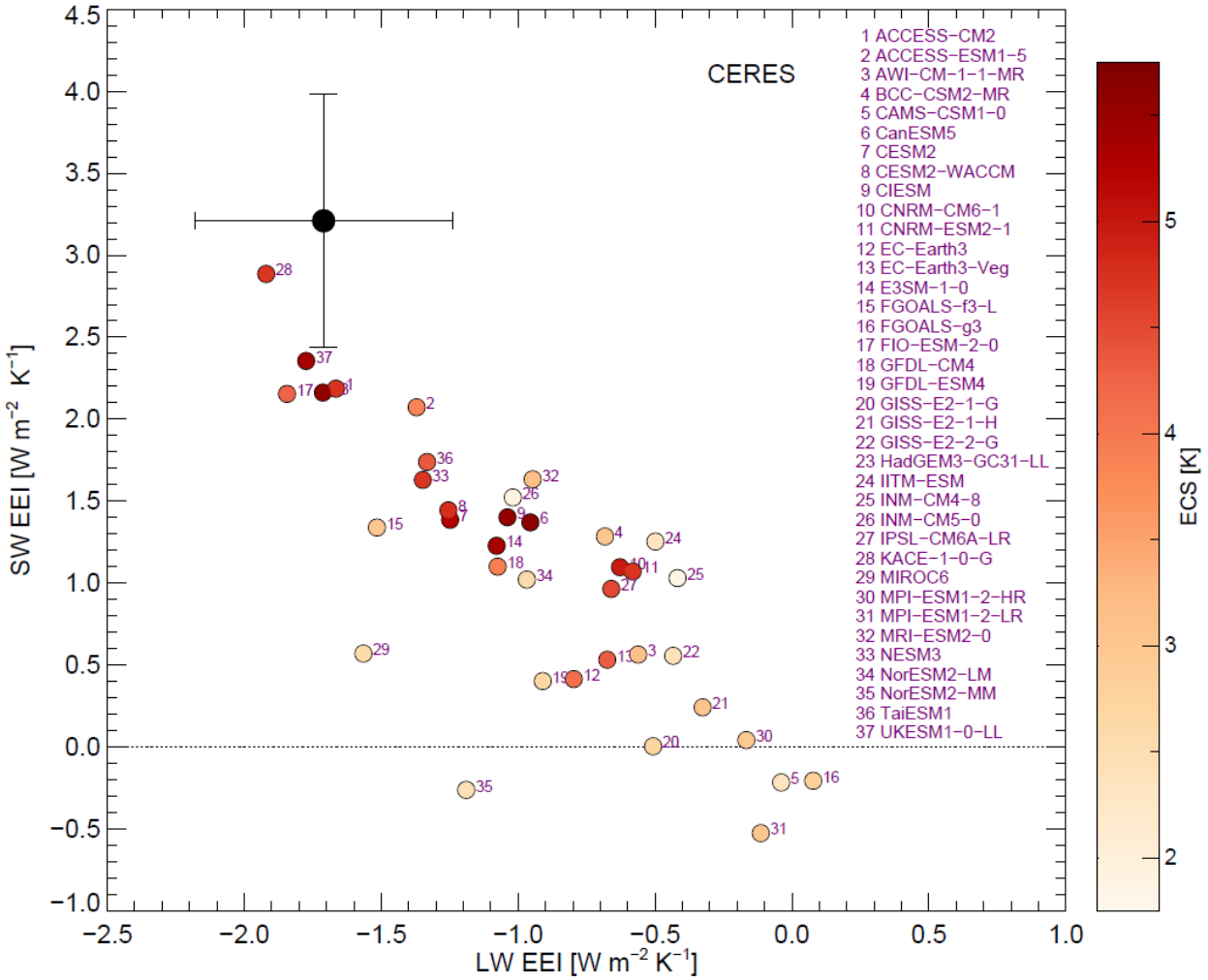

Fig 4: SW EEI per degree warming trends versus LW EEI trends per degree warming in CMIP6 models and CERES satellite data. Colours show climate sensitivity of each CMIP6 model. Temperature for the CERES data is taken from GISTEMP (*32*). Lines around the CERES trends are 90% confidence intervals.

1. R. Knutti, M. A. A. Rugenstein, G. C. Hegerl, Beyond equilibrium climate sensitivity. *Nature Geosci.* **10**, 727–736 (2017).
2. J. Hansen *et al.*, Climate Impact of Increasing Atmospheric Carbon Dioxide. *Science* **213**, 957-966 (1981).
3. G. H. Roe, M. B. Baker, Why is climate sensitivity so unpredictable? *Science* **318**, 629-632 (2007).
4. P. Forster *et al.*, "The Earth's Energy Budget, Climate Feedbacks, and Climate Sensitivity. In Climate Change 2021: The Physical Science Basis. Contribution of Working Group I to the Sixth Assessment Report of the Intergovernmental Panel on Climate Change " (Cambridge University Press., 2021).
5. S. C. Sherwood *et al.*, An Assessment of Earth's Climate Sensitivity Using Multiple Lines of Evidence. *Rev. Geophys.* **58**, e2019RG000678 (2020).
6. P. Ceppi, P. Nowack, Observational evidence that cloud feedback amplifies global warming. *Proceedings of the National Academy of Sciences* **118**, e2026290118 (2021).
7. G. V. Cesana *et al.*, Observational constraint on a feedback from supercooled clouds reduces projected warming uncertainty. *Communications Earth & Environment* **5**, 181 (2024).
8. I. Tan, T. Storelvmo, M. D. Zelinka, Observational constraints on mixed-phase clouds imply higher climate sensitivity. *Science* **352**, 224-227 (2016).
9. R. Vogel *et al.*, Strong cloud–circulation coupling explains weak trade cumulus feedback. *Nature* **612**, 696-700 (2022).
10. A. Modak, T. Mauritsen, The 2000–2012 Global Warming Hiatus More Likely With a Low Climate Sensitivity. *Geophys. Res. Lett.* **48**, e2020GL091779 (2021).
11. D. Olonscheck, M. Rugenstein, Coupled Climate Models Systematically Underestimate Radiation Response to Surface Warming. *Geophys. Res. Lett.* **51**, e2023GL106909 (2024).
12. K. C. Armour *et al.*, Sea-surface temperature pattern effects have slowed global warming and biased warming-based constraints on climate sensitivity. *Proceedings of the National Academy of Sciences* **121**, e2312093121 (2024).
13. J. Quaas *et al.*, Robust evidence for reversal of the trend in aerosol effective climate forcing. *Atmos. Chem. Phys.* **22**, 12221-12239 (2022).
14. P. M. Forster *et al.*, Indicators of Global Climate Change 2022: annual update of large-scale indicators of the state of the climate system and human influence. *Earth Syst. Sci. Data* **15**, 2295-2327 (2023).
15. N. G. Loeb *et al.*, Satellite and Ocean Data Reveal Marked Increase in Earth's Heating Rate. *Geophys. Res. Lett.* **48**, e2021GL093047 (2021).
16. Ø. Hodnebrog *et al.*, Recent reductions in aerosol emissions have increased Earth's energy imbalance. *Communications Earth & Environment* **5**, 166 (2024).
17. J. E. Hansen *et al.*, Global warming in the pipeline. *Oxford Open Climate Change* **3**, (2023).
18. G. A. Schmidt *et al.*, CERESMIP: a climate modeling protocol to investigate recent trends in the Earth's Energy Imbalance. *Frontiers in Climate* **5**, (2023).
19. V. Eyring *et al.*, Overview of the Coupled Model Intercomparison Project Phase 6 (CMIP6) experimental design and organization. *Geosci. Model Dev.* **9**, 1937-1958 (2016).
20. Z. Li, M. H. England, S. Groeskamp, Recent acceleration in global ocean heat accumulation by mode and intermediate waters. *Nature Communications* **14**, 6888 (2023).

21. A. Minière, K. von Schuckmann, J.-B. Sallée, L. Vogt, Robust acceleration of Earth system heating observed over the past six decades. *Scientific Reports* **13**, 22975 (2023).
22. K. von Schuckmann *et al.*, Heat stored in the Earth system 1960–2020: where does the energy go? *Earth Syst. Sci. Data* **15**, 1675-1709 (2023).
23. N. G. Loeb *et al.*, Observational Assessment of Changes in Earth's Energy Imbalance Since 2000. *Surv. Geophys.*, 10.1007/s10712-10024-09838-10718 (2024).
24. A. Duspayev, M. G. Flanner, A. Riihelä, Earth's Sea Ice Radiative Effect From 1980 to 2023. *Geophys. Res. Lett.* **51**, e2024GL109608 (2024).
25. A. Donohoe, K. C. Armour, A. G. Pendergrass, D. S. Battisti, Shortwave and longwave radiative contributions to global warming under increasing CO2. *Proc. Natl. Acad. Sci. U.S.A.* **111**, 16700-16705 (2014).
26. J. M. Gregory *et al.*, A new method for diagnosing radiative forcing and climate sensitivity. *Geophys. Res. Lett.* **31**, L03205 (2004).
27. M. D. Zelinka *et al.*, Causes of Higher Climate Sensitivity in CMIP6 Models. *Geophys. Res. Lett.* **47**, e2019GL085782 (2020).
28. M. Rugenstein *et al.*, Connecting the SST Pattern Problem and the Hot Model Problem. *Geophys. Res. Lett.* **50**, e2023GL105488 (2023).
29. V. Ramanathan *et al.*, Cloud-Radiative Forcing and Climate: Results from the Earth Radiation Budget Experiment. *Science* **243**, 57-63 (1989).
30. C. J. Smith *et al.*, Effective radiative forcing and adjustments in CMIP6 models. *Atmos. Chem. Phys.* **20**, 9591-9618 (2020).
31. P. M. Forster *et al.*, Indicators of Global Climate Change 2023: annual update of key indicators of the state of the climate system and human influence. *Earth Syst. Sci. Data* **16**, 2625-2658 (2024).
32. N. J. L. Lenssen *et al.*, Improvements in the GISTEMP Uncertainty Model. *J. Geophys. Res. - Atmos.* **124**, 6307-6326 (2019).
33. A. Singh, K. Gaurav, G. K. Meena, S. Kumar, Estimation of Soil Moisture Applying Modified Dubois Model to Sentinel-1; A Regional Study from Central India. *Remote Sensing* **12**, 2266 (2020).

Supplementary Materials for

Observed trend in Earth energy imbalance provides a constraint for low climate sensitivity models

Gunnar Myhre, Øivind Hodnebrog, Norman Loeb, Piers M. Forster

Corresponding author: gunnar.myhre@cicero.oslo.no

The PDF file includes:

Supplementary Text
Figs. S1 to S6
Tables S1 to S2

Supplementary Text

AMIP-simulations

We have included additional climate model simulations that use observed monthly sea-surface temperatures and sea-ice concentration for 2001-2019 (gray symbols in Figure 3a-b). These simulations are described in Hodnebrog et al. (*16*). In brief, most simulations use anthropogenic aerosol (precursor) emissions from the Community Emissions Data System (CEDS) version of April 2021, while other forcings follow the CMIP6 historical setup until 2014 and assume SSP2-4.5 thereafter. These simulations (BASE) are included in Figure 3b, while simulations with constant aerosol emissions (AERO2000) and with all climate drivers constant (ALL2000) are included in Figure 3a.

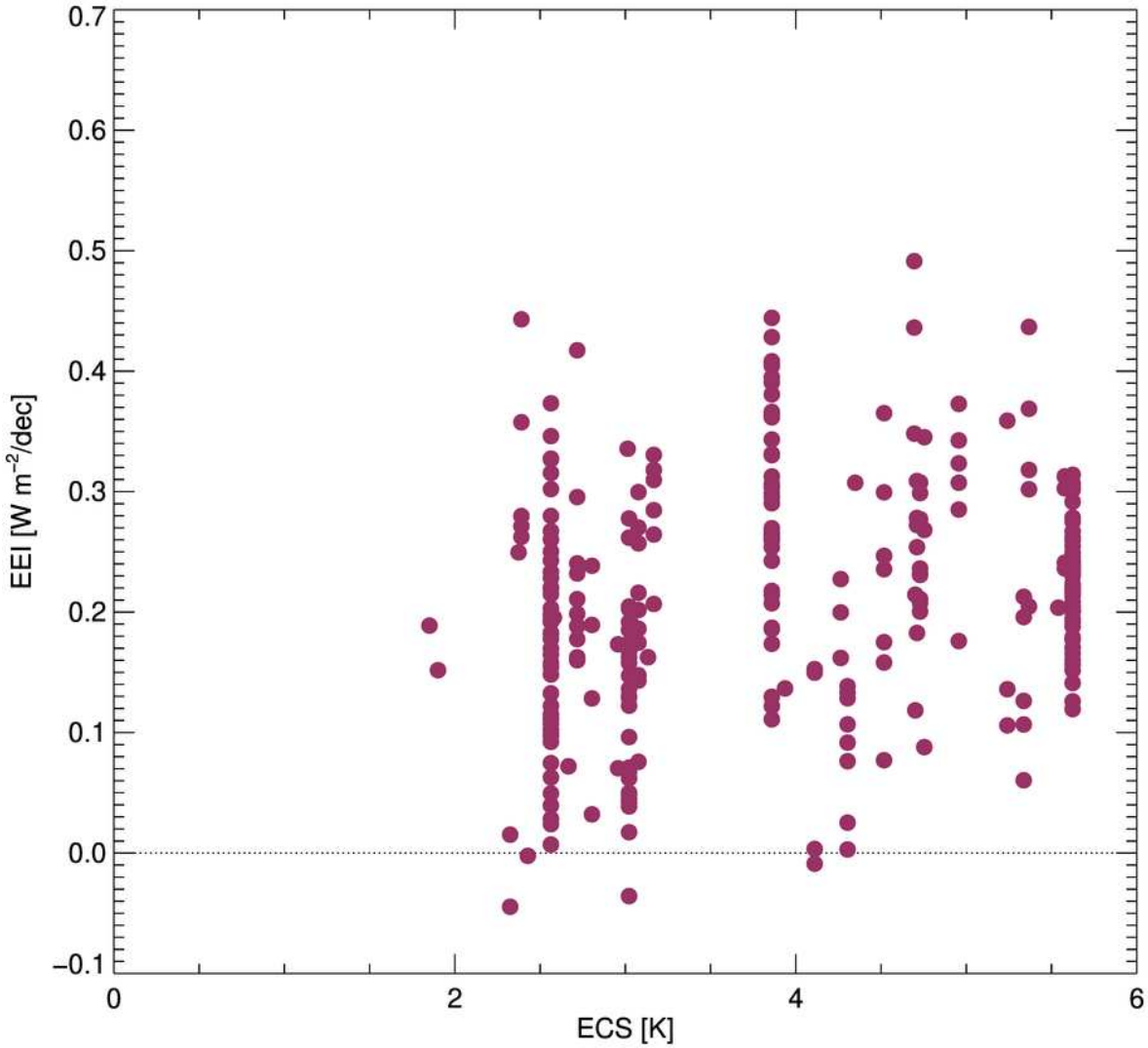

Fig. S1. Trends in net EEI (for the period 2001-2023) as a function of climate sensitivity (ECS) in CMIP6 simulations.

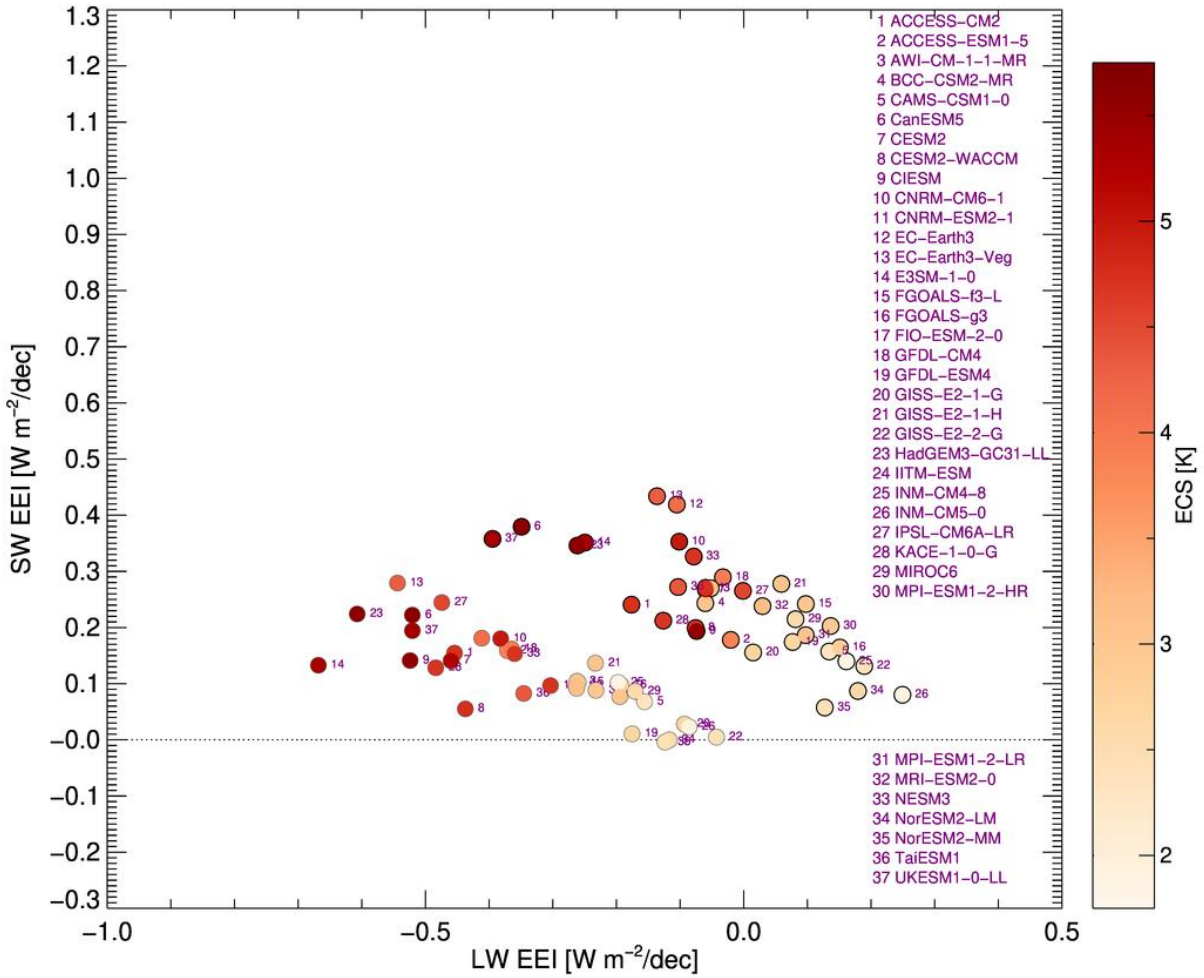

Fig. S2. Trends in clear sky LW and SW EEI in 1pctCO2 and abrupt4xCO2 simulations. Colours show the climate sensitivity of each CMIP6. X-and y-axes are the same as in Figure 3a. Results for the 1pctCO2 simulations have thicker lines around the circles than the abrupt-4xCO2 simulations.

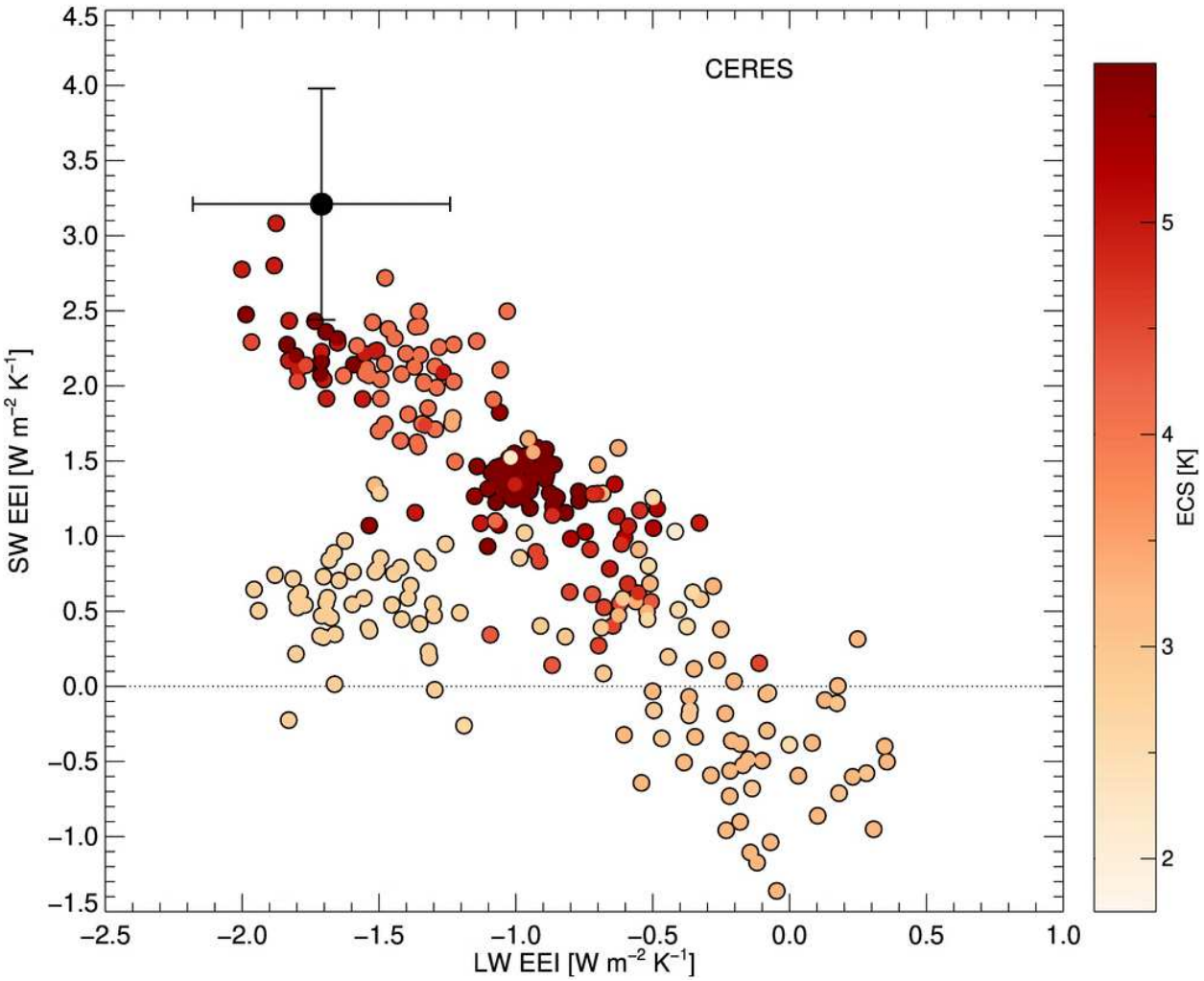

Fig. S3. SW EEI per degree warming trends versus LW EEI trends per degree warming in CMIP6 models and CERES satellite data. Colours show climate sensitivity of each CMIP6 model. All individual ensemble members from CMIP6 models are included.

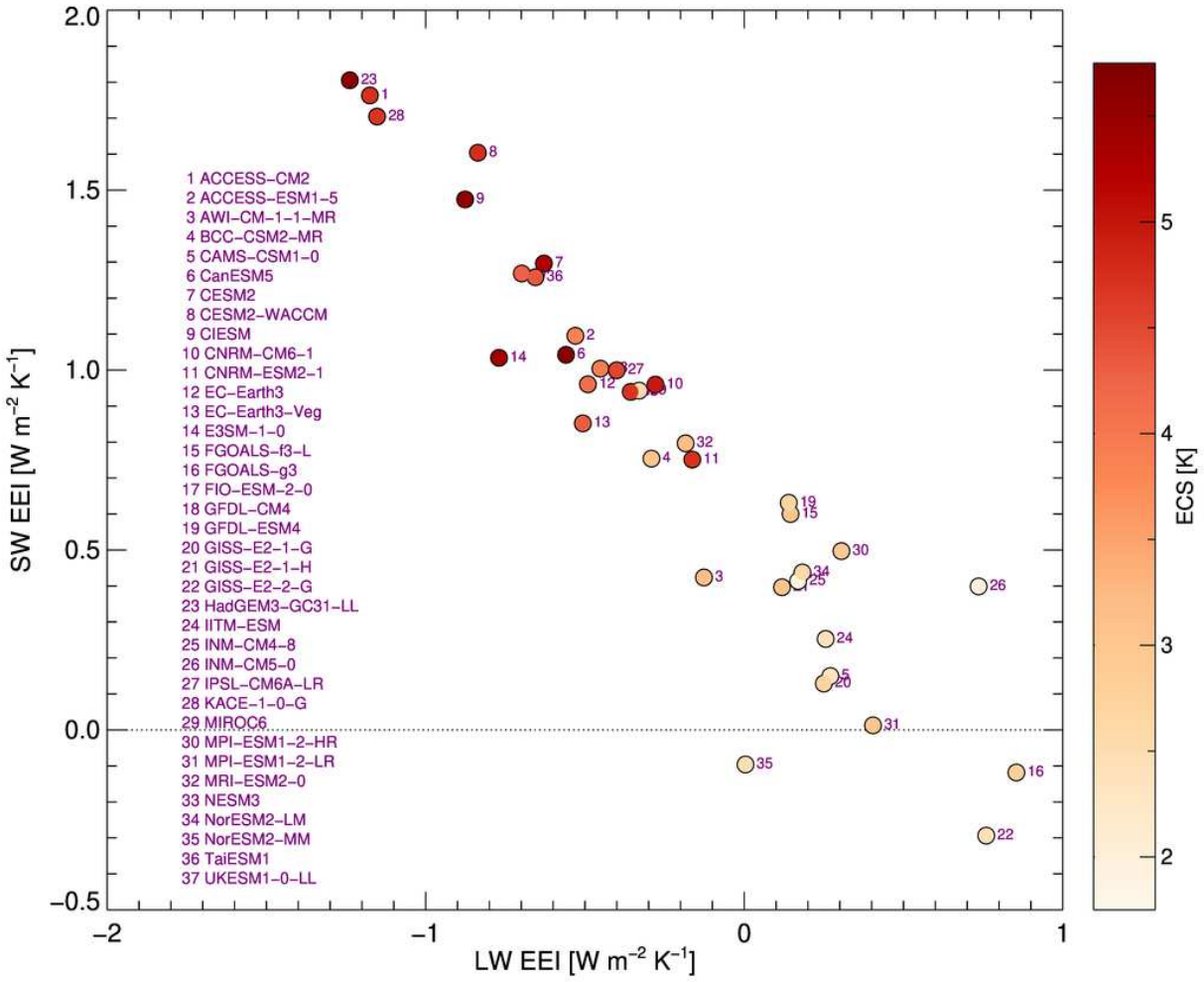

Fig. S4. Trends in all-sky LW and SW EEI per degree of warming in the CMIP6 experiment 1pctCO2. Colours show the climate sensitivity of each CMIP6 model.

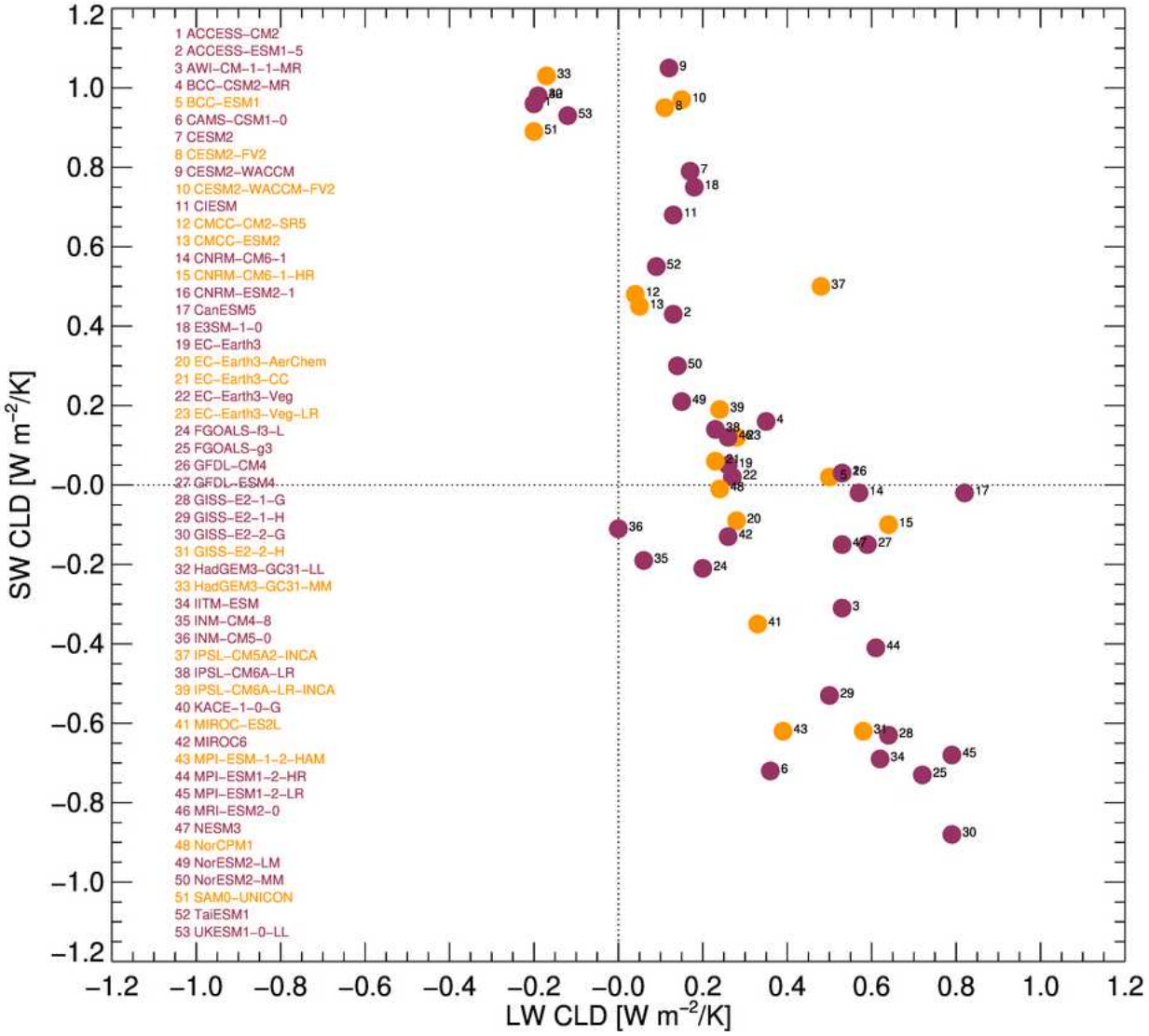

Fig. S5. LW and SW cloud feedbacks derived in Zelinka et al. (*27*). Models in orange colours are not included elsewhere in this study.

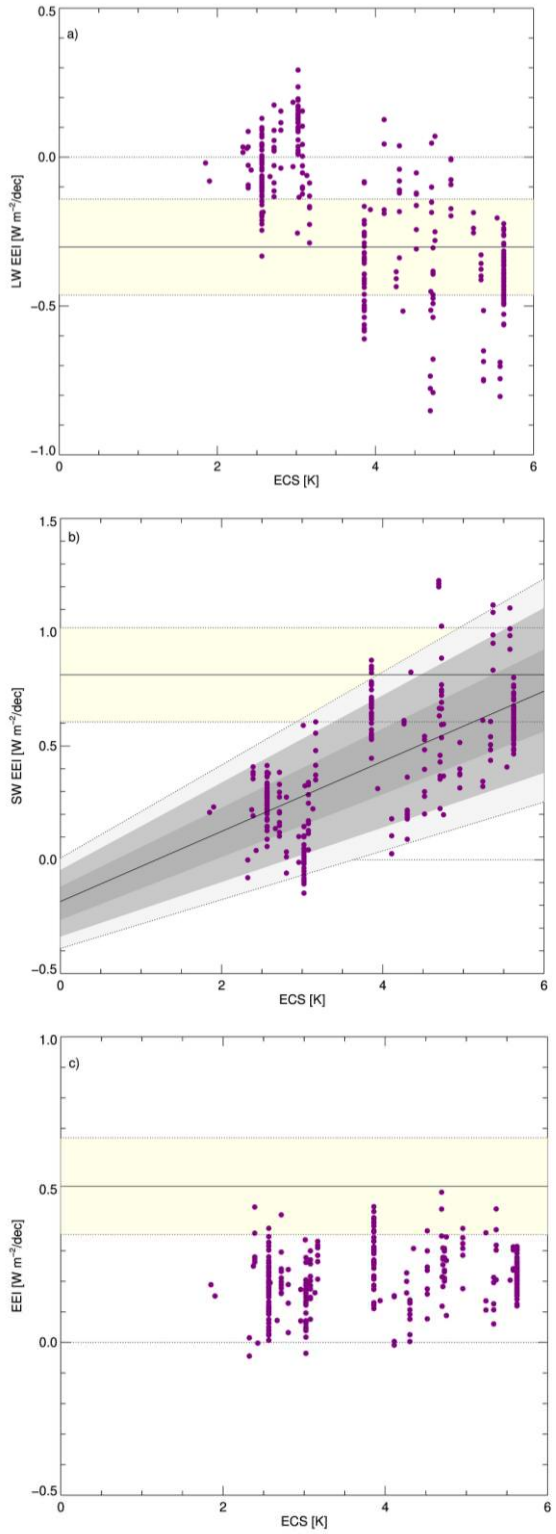

Fig. S6. LW, SW, and net EEI trends for 2001 to 2023 versus ECS in CMIP6 models. The CERES data for 2001 to 2023 is shown with a solid line and yellow shading for the 90% confidence interval (CI). For the SW EEI trends, linear regressions are shown by a solid line with 90% CI in dark grey, 99.9% CI in grey and 99.999% CI in light grey.

Table S1. List of CMIP6 models included in the study with number of ensemble members and climate sensitivity (effective climate sensitive with regression of 150 years).

# in figures	Model	#Members	Climate sensitivity
1	ACCESS-CM2	10	4.73
2	ACCESS-ESM1-5	40	3.86
3	AWI-CM-1-1-MR	1	3.13
4	BCC-CSM2-MR	1	3.03
5	CAMS-CSM1-0	2	2.32
6	CanESM5	50	5.62
7	CESM2	3	5.24
8	CESM2-WACCM	3	4.75
9	CIESM	1	5.54
10	CNRM-CM6-1	6	4.96
11	CNRM-ESM2-1	5	4.71
12	EC-Earth3	4	4.11
13	EC-Earth3-Veg	8	4.30
14	E3SM-1-0	5	5.34
15	FGOALS-f3-L	1	3.01
16	FGOALS-g3	4	2.80
17	FIO-ESM-2-0	3	4.26
18	GFDL-CM4	1	3.94
19	GFDL-ESM4	1	2.67
20	GISS-E2-1-G	10	2.72
21	GISS-E2-1-H	10	3.08
22	GISS-E2-2-G	5	2.39
23	HadGEM3-GC31-LL	4	5.58
24	IITM-ESM	1	2.37
25	INM-CM4-8	1	1.85
26	INM-CM5-0	1	1.90
27	IPSL-CM6A-LR	7	4.52
28	KACE-1-0-G	3	4.69
29	MIROC6	50	2.56
30	MPI-ESM1-2-HR	2	2.96
31	MPI-ESM1-2-LR	30	3.02
32	MRI-ESM2-0	6	3.17
33	NESM3	2	4.70
34	NorESM2-LM*	1	2.58
35	NorESM2-MM	1	2.43
36	TaiESM1	1	4.35
37	UKESM1-0-LL	5	5.37

*NorESM2-LM has a negative EEI in the period 2001-2005 in the historical simulation connected to the SSP585 ensemble. We have used the only historical ensemble member for NorESM2-LM which has a positive EEI for the same period, which is connected to a SSP245 ensemble member. All other models included in this study have a positive EEI in the period 2001-2005, consistent with observational data.

Table S2. Regression coefficients for SW EEI in Fig S5, derived using the method from Singh, Gaurav, Meena and Kumar (*33*). Upper and lower values given for 90%, 99.9% and 99.999% CI.

CI	Constants	Coefficients
50%	-0.183	0.154
90%	-0.118 / -0.264	0.174 / 0.138
99.9%	-0.045 / -0.338	0.192 / 0.120
99.999%	0.007 / -0.389	0.205 / 0.107

5